The Astrophysical Journal, 837:104 (11pp), 2017 March 10 https://doi.org/10.3847/1538-4357/aa6043

Electric Current Filamentation Induced by 3D Plasma Flows in the Solar Corona

Dieter H. Nickeler[1], Thomas Wiegelmann[2], Marian Karlický[1], and Michaela Kraus[1,3]
[1] Astronomický ústav, Akademie věd České Republiky, v.v.i., Fričova 298, 251 65 Ondřejov, Czech Republic; dieter.nickeler@asu.cas.cz
[2] Max-Planck Institut für Sonnensystemforschung, Justus-von-Liebig-Weg 3, D-37077 Göttingen, Germany
[3] Tartu Observatory, 61602 Tõravere, Tartumaa, Estonia
Received 2017 January 16; revised 2017 February 9; accepted 2017 February 10; published 2017 March 8

Abstract

Many magnetic structures in the solar atmosphere evolve rather slowly, so they can be assumed as (quasi-)static or (quasi-)stationary and represented via magnetohydrostatic (MHS) or stationary magnetohydrodynamic (MHD) equilibria, respectively. While exact 3D solutions would be desired, they are extremely difficult to find in stationary MHD. We construct solutions with magnetic and flow vector fields that have three components depending on all three coordinates. We show that the noncanonical transformation method produces quasi-3D solutions of stationary MHD by mapping 2D or 2.5D MHS equilibria to corresponding stationary MHD states, that is, states that display the same field-line structure as the original MHS equilibria. These stationary MHD states exist on magnetic flux surfaces of the original 2D MHS states. Although the flux surfaces and therefore also the equilibria have a 2D character, these stationary MHD states depend on all three coordinates and display highly complex currents. The existence of geometrically complex 3D currents within symmetric field-line structures provides the basis for efficient dissipation of the magnetic energy in the solar corona by ohmic heating. We also discuss the possibility of maintaining an important subset of nonlinear MHS states, namely force-free fields, by stationary flows. We find that force-free fields with nonlinear flows only arise under severe restrictions of the field-line geometry and of the magnetic flux density distribution.

Key words: magnetohydrodynamics (MHD) – methods: analytical – Sun: corona – Sun: flares

1. Introduction

Many structures in the atmosphere of the Sun and in solar-type stars evolve on relatively large timescales, so they can be described within the frame of quasi-stationary or quasi-static magnetohydrodynamics (MHD). Prominent examples are solar arcade structures, loops, and prominences. To represent them, typically magnetohydrostatic (MHS) equilibria (e.g., Low 1982; Solov'ev & Kirichek 2015) or stationary-state models, that is, stationary MHD equilibria, are calculated (e.g., Petrie & Neukirch 1999; Petrie et al. 2005).

Generally, it would be desirable to have a full 3D representation of the MHD equilibrium states. However, as was already mentioned by Parker (1972), it is normally not possible to construct 3D states in the functional vicinity of 2D states. This means that 2D equilibria on which perturbations are imposed typically do not relax into smooth 3D states (Tsinganos 1982). Instead, the resulting equilibria must contain tangential discontinuities, that is, singular current sheets. This is known as Parker's conjecture (Parker 1983a, 1983b, 1988), which states that no regular equilibria exist without a symmetry. In this context, symmetry does not necessarily imply that the system has an ignorable coordinate (Low 1985), where ignorable coordinate means that in a specific coordinate system the physical values do not depend on this coordinate. We note that under specific circumstances a few regular classes of 3D MHS states have been found (see, e.g., Low 1982; Neukirch 1995), and a set of exact analytical 3D stationary MHD flows exists as well (see, e.g., Bogoyavlenskij 2001, 2002). However, the computation of these solutions requires that a complete stationary flow must already be known.

According to Parker, the appearance of singular current sheets could provide a suitable mechanism for acceleration and heating of the coronal plasma via ohmic heating, i.e., joule dissipation, caused by magnetic reconnection within these current sheets. To guarantee that heating is provided on a regular basis (i.e., also during times with no huge eruptions), successive heating should take place. This can only be achieved considering quasi-continuous small-scale eruptions, the so-called nanoflares (Parker 1988). However, it is still highly debated whether large-scale eruptions or small-scale nanoflares are the major mechanism for the heating of the solar coronal plasma (see, e.g., Parnell & de Moortel 2012; Švanda & Karlický 2016).

Shearing motions of the magnetic field lines, such as at the footpoints of arcade structures, can be used to produce nanoflares (see, e.g., Bingert & Peter 2011; Bourdin et al. 2013; Hansteen et al. 2015) or large-scale eruptions (e.g., Manchester 2003; Kotrč et al. 2013; Toriumi et al. 2013; Leake et al. 2014). Such a procedure does not necessarily converge into an equilibrium state anymore. Therefore, in numerical simulations, these sheared field lines might be forced to relax into an equilibrium state by introducing numerical resistivities and viscosities (e.g., Wilmot-Smith et al. 2011; Prior & Yeates 2016).

Another approach for small-scale eruptions and heating was made by Pongkitiwanichakul et al. (2015), who applied a so-called volumetric Parker model. This model is not based on the shearing motions of the footpoints. Instead, a large-scale motion of the magnetic field lines is applied throughout the volume of the fluid. This large-scale motion is driven by an initial stationary flow, generated by a time-dependent stream function whose Fourier components are kept fixed at each time step. These stationary flows generate additional turbulent flows, which are allowed to evolve in time.

Alternatively, a model including self-consistent plasma flows was developed by Nickeler et al. (2013, 2014). This model produces highly fragmented, strongly peaked currents and

vortices spreading from large to small scales, while the system remains in a well-defined equilibrium.

In most of the aforementioned approaches, the initial condition is either a static or some arbitrary field that is not compatible with the resulting flow field. The numerically calculated corresponding changes of the fields are, therefore, based either on linear or nonlinear perturbation theory or on stochastics. What is often neglected is that observations imply stationary flows in active regions and coronal holes rather than pure force-free or static fields (Winebarger et al. 2001, 2002; Marsch et al. 2004; Wiegelmann et al. 2005). Also, during preflare stages, upflows in the photosphere and flows along loops were observed (e.g., Yoshimura et al. 1971; Harvey & Harvey 1976; Wallace et al. 2010). Hence, an initial condition including stationary flows, as was presented by Nickeler & Wiegelmann (2010, 2012), seems more appropriate.

Nonlinear MHD flow models for loops, sunspots, and magnetic arcade structures exist (see, e.g., Tsinganos et al. 1993; Petrie & Neukirch 1999; Petrie et al. 2002, 2005), but they were not developed explicitly for the purpose of explaining coronal heating. Nevertheless, nonlinear MHD theory provides the proper tool for particle acceleration via generation of electric fields in a slightly nonideal/resistive environment and, therefore, for local heating processes (Nickeler et al. 2014).

In this paper, we wish to reinforce Parker's conjecture of heating via multiple current sheets and multiple reconnection sites. In connection with the equilibrium problem introduced by Parker (1972), we need therefore a proper method that allows slight deviations from symmetric 2D to (almost) 3D structures. The known magnetic flux densities and the corresponding derived currents obtained from observations are far below the threshold for sufficient dissipation of magnetic energy in general, i.e., joule heating by extremely strong currents in the case of, for example, Spitzer resistivity, or the threshold for anomalous resistivity to trigger magnetic reconnection. This implies that the current density on these scales is too low to produce current-driven microinstabilities. However, the observed large-scale fields might display steep gradients on smaller scales. Complex flow patterns and steep gradients in active regions indicate the existence of shear flows, as was reported by Marsch et al. (2004). The changing of the magnetic field structure often seems to coincide with sharp changes in the flows. Hence, this trend might be expected to continue when going to even smaller, yet-unresolved scales.

For a better comprehension of ohmic heating and acceleration of plasma and particles, we need more detailed information about current sheet structures in the solar atmosphere. While both observations and numerical simulations currently cannot resolve small-scale structures, an analytical approach is a useful physical approximation that provides detailed information down to the theoretical dissipation scales, which are for solar corona conditions below 10 m. Based on the noncanonical transformation method developed by Gebhardt & Kiessling (1992) and utilized by, for example, Cicogna & Pegoraro (2015), we will show that there is a connection between the breaking of the symmetry and the down-cascading of the current sheet scales. The breaking of the symmetry is done by field-aligned flows that have a strong gradient perpendicular to the field lines. These flows cause strong gradients of the magnetic field strength normal to the field lines, implying small-scale current sheets.

2. Problem Description and Basic Assumptions

The magnetic field structures in the solar atmosphere, especially in the corona, resemble magnetic arches and also closed field-line structures emulating flux ropes, surrounded by bundles of open field lines. These magnetic structures form the stage on which chromospheric and coronal heating takes place. For a reasonable representation of these structures, it is necessary to calculate the nonlinear fields forming the magnetic scaffold in the frame of stationary MHD.

2.1. Stationary MHD Equations

We focus on incompressible field-aligned sub-Alfvénic flows, because they are exclusively related to MHS states. This has been proved by Gebhardt & Kiessling (1992), Nickeler et al. (2006), and Nickeler & Wiegelmann (2010), who found that only incompressible field-aligned MHD flows can be unambiguously reduced to MHS-type equations. MHS equilibria are therefore an infinitesimally small subset of field-aligned incompressible flows.

Another advantage of field-aligned flows is that they guarantee that, according to ideal Ohm's law, the electric field in ideal MHD vanishes,

$$\boldsymbol{E} + \boldsymbol{v} \times \boldsymbol{B} = 0 \quad \Rightarrow \quad \boldsymbol{E} = 0, \tag{1}$$

and, therefore, fulfills automatically the condition that the electric field is stationary.

To simplify the representation of the equations, we introduce normalized parameters. These require the definition of normalization constants $\hat{B}$, $\hat{\rho}$, $\hat{l}$, $\hat{v}_{\rm A}$, and $\hat{p}$. Let $\boldsymbol{v}$ be the plasma velocity normalized by the normalized Alfvén velocity $\hat{v}_{\rm A} = \hat{B}/\sqrt{\mu_0 \hat{\rho}}$, ρ the mass density normalized by $\hat{\rho}$, $\boldsymbol{j} = \boldsymbol{\nabla} \times \boldsymbol{B}$ the current density vector normalized by $\hat{B}/(\mu_0 \hat{l})$ with $\hat{l}$ as the characteristic length scale, and p the scalar plasma pressure normalized by $\hat{p} = \hat{B}^2/\mu_0$. Hence, the set of equations of stationary, field-aligned incompressible MHD, consisting of the mass continuity equation, the Euler equation, the definition for field-aligned flow and Alfvén Mach number $M_{\rm A}$, the incompressibility condition, and the solenoidal condition for the magnetic field, can be written in the following form:

$$\boldsymbol{\nabla} \cdot (\rho \boldsymbol{v}) = 0, \tag{2}$$

$$\rho (\boldsymbol{v} \cdot \boldsymbol{\nabla}) \boldsymbol{v} = \boldsymbol{j} \times \boldsymbol{B} - \boldsymbol{\nabla} p, \tag{3}$$

$$\boldsymbol{v} = \frac{M_{\rm A} \boldsymbol{B}}{\sqrt{\rho}}, \tag{4}$$

$$\boldsymbol{\nabla} \cdot \boldsymbol{v} = 0, \tag{5}$$

$$\boldsymbol{\nabla} \cdot \boldsymbol{B} = 0. \tag{6}$$

The combination of Equations (5) and (4) yields the conserved values, $\boldsymbol{B} \cdot \boldsymbol{\nabla} \rho = 0$ and $\boldsymbol{B} \cdot \boldsymbol{\nabla} M_{\rm A} = 0$, and therefore also $\boldsymbol{v} \cdot \boldsymbol{\nabla} \rho = 0$ and $\boldsymbol{v} \cdot \boldsymbol{\nabla} M_{\rm A} = 0$. Consequently, the Alfvén Mach number and the density are constant along field lines, and the magnetic and the velocity field are integrable, i.e., nonergodic (Grad & Rubin 1958; Stern 1970).

Integrable, divergence-free fields, such as the magnetic field, can be represented by so-called Euler or Clebsch potentials, f and g, via the form

$$\boldsymbol{B} = \boldsymbol{\nabla} f \times \boldsymbol{\nabla} g. \tag{7}$$

In general, these Euler potentials are functions of all three coordinates x, y, z. The representation can also be made by alternative Euler potentials, say α and β, if these are related to the original ones via the mapping $\alpha = \alpha(f, g)$ and $\beta = \beta(f, g)$, and if, in addition, the Poisson bracket is identical to unity, meaning that

$$[\alpha, \beta]_{f,g} \coloneqq \frac{\partial \alpha}{\partial f}\frac{\partial \beta}{\partial g} - \frac{\partial \alpha}{\partial g}\frac{\partial \beta}{\partial f} \equiv 1. \tag{8}$$

Then the field remains unchanged and can be written as

$$\boldsymbol{B} = \boldsymbol{\nabla} f \times \boldsymbol{\nabla} g = \boldsymbol{\nabla}\alpha \times \boldsymbol{\nabla}\beta = [\alpha, \beta]_{f,g}\, \boldsymbol{\nabla} f \times \boldsymbol{\nabla} g. \tag{9}$$

This kind of transformation is called canonical transformation.

A noncanonical and hence "active" transformation, on the other hand, is performed in case the Poisson bracket is not identical to unity. It was shown by Gebhardt & Kiessling (1992) that such an active transformation reflects the similarity between MHS states and stationary states in incompressible MHD. This can be seen from the following.

If we start from the momentum equation of MHS given by

$$\boldsymbol{\nabla} p_S = \boldsymbol{j}_S \times \boldsymbol{B}_S = (\boldsymbol{\nabla} \times \boldsymbol{B}_S) \times \boldsymbol{B}_S \tag{10}$$

and represent the MHS magnetic field, $\boldsymbol{B}_S$, via the Euler potentials f and g (where in the following the Euler potentials f and g refer to MHS fields and α and β to stationary MHD fields),

$$\boldsymbol{B}_S = \boldsymbol{\nabla} f \times \boldsymbol{\nabla} g, \tag{11}$$

then the MHS pressure, p_S, can always be written locally as an explicit function of f and g:

$$p_S = p_S(f, g). \tag{12}$$

Let us now assume we know a solution $(p_S, \boldsymbol{B}_S)$ for Equation (10) in which the magnetic field and the pressure are given in the form of the Equations (11) and (12). If we additionally define a relation between the Alfvén Mach number M_A and the Poisson bracket of the form

$$([f, g]_{\alpha,\beta})^2 \equiv 1 - M_\mathrm{A}^2 > 0 \tag{13}$$

or, equivalently,

$$([\alpha, \beta]_{f,g})^2 \equiv \frac{1}{1 - M_\mathrm{A}^2} \geqslant 1, \tag{14}$$

where M_A can always be regarded as an explicit function of α and β (or f and g) bounded by one, then

$$\boldsymbol{B} = \boldsymbol{\nabla}\alpha \times \boldsymbol{\nabla}\beta \tag{15}$$

can be considered as a magnetic field of a stationary MHD equilibrium. This means that the corresponding velocity field can be written as

$$\boldsymbol{v} = \frac{M_\mathrm{A}\boldsymbol{B}}{\sqrt{\rho}}, \tag{16}$$

while the magnetic field, the corresponding current density, and the plasma pressure take the form

$$\boldsymbol{B} = [\alpha, \beta]_{f,g}\, \boldsymbol{B}_S \equiv \frac{\boldsymbol{B}_S}{\sqrt{1 - M_\mathrm{A}^2}}, \tag{17}$$

$$\boldsymbol{j} = \frac{M_\mathrm{A}\, \boldsymbol{\nabla} M_\mathrm{A} \times \boldsymbol{B}_S}{(1 - M_\mathrm{A}^2)^{3/2}} + \frac{\boldsymbol{j}_S}{(1 - M_\mathrm{A}^2)^{1/2}}, \tag{18}$$

$$p = p_S - \frac{1}{2}\rho \boldsymbol{v}^2 \tag{19}$$

for sub-Alfvénic flows, and

$$\boldsymbol{B} = [\alpha, \beta]_{f,g}\, \boldsymbol{B}_S \equiv \frac{\boldsymbol{B}_S}{\sqrt{M_\mathrm{A}^2 - 1}}, \tag{20}$$

$$\boldsymbol{j} = -\frac{M_\mathrm{A}\, \boldsymbol{\nabla} M_\mathrm{A} \times \boldsymbol{B}_S}{(M_\mathrm{A}^2 - 1)^{3/2}} + \frac{\boldsymbol{j}_S}{(M_\mathrm{A}^2 - 1)^{1/2}}, \tag{21}$$

$$p = p_0 - p_S - \frac{1}{2}\rho \boldsymbol{v}^2 \tag{22}$$

for super-Alfvénic flows, implying that the stationary MHD equations (Equations (2)–(6)) are fulfilled. The parameter p_0 represents here a pressure offset, necessary to avoid negative pressure values and to provide boundary conditions. In any case, the plasma density, ρ, and the Alfvénic Mach number are explicit functions of the Euler potentials f and g. If these can be constrained by reasonable boundary conditions (e.g., from observations), the velocity and pressure, and correspondingly the complete stationary equilibrium, can be calculated from a known solution of p_S and $\boldsymbol{B}_S$. One property of the transformation is that the geometrical and topological field-line structures of the initial MHS state remain unchanged. A second one is that the flow induces current fragmentation whereby the flow itself is generated via variations of the pressure. Current fragmentation induced by pressure pulses that originate close to magnetic null points was also reported by Jelínek et al. (2015).

2.2. General Parameterization of the Transformation

In the previous section we showed that a transformation method exists. What is needed next is to find a way to calculate explicitly the transformation from the initial potentials f and g to the final ones α and β.

The sub-Alfvénic Poisson bracket relation Equation (14) and, therefore, also the sub-Alfvénic M_A can generally be represented via

$$M_\mathrm{A} \equiv \tanh \mathcal{M}(f, g)$$
$$([\alpha, \beta]_{f,g})^2 \equiv \frac{1}{1 - M_\mathrm{A}^2} \equiv (\cosh \mathcal{M}(f, g))^2 \geqslant 1. \tag{23}$$

The function $\mathcal{M}$ should be at least twice continuously differentiable. The condition Equation (23) guarantees that the Alfvén Mach number is bounded by one. Keeping the polarity of the mapped magnetic field (see Equation (9)), Equation (23) results in a linear partial differential equation for α and β as functions of f and g:

$$[\alpha, \beta]_{f,g} \coloneqq \frac{\partial \alpha}{\partial f}\frac{\partial \beta}{\partial g} - \frac{\partial \alpha}{\partial g}\frac{\partial \beta}{\partial f} \equiv \cosh \mathcal{M}(f, g), \tag{24}$$

which could basically be solved based on the method of characteristics.

Searching for a method to reduce Equation (24) to a generally simpler form can be done by assuming without loss

of generality

$$\alpha_0 = \alpha_0(f), \tag{25}$$

$$\beta_0 = \left(\frac{d\alpha_0}{df}\right)^{-1} \int \cosh \mathcal{M}(f, g)\, dg + \beta_{00}(f), \tag{26}$$

which automatically satisfies Equation (24). The functions $\alpha_0(f)$ and $\beta_{00}(f)$ can be chosen arbitrarily to satisfy boundary conditions and constraints for the magnetic and the velocity fields. All equivalent transformations $\alpha = \alpha(f, g)$ and $\beta = \beta(f, g)$ can be found by corresponding canonical transformations of α_0 and β_0.

2.3. Basic Equations for 2D and 2.5D MHS Equilibria

The general solution for stationary equilibria presented in the previous section is valid in all dimensions. Ideally, 3D stationary equilibria would be desired. Computing such equilibria via the transformation method requires the knowledge of exact and analytical 3D MHS equilibria. However, only a few such 3D MHS equilibria are known (Low 1991; Neukirch 1995, 1997; Petrie & Neukirch 1999). Nevertheless, for many practical scenarios, the field geometry displays some symmetry. Translationally invariant equilibria serve as examples. These can be associated, for example, with arcade structures above the polarity inversion line (PIL). These PILs resemble the z axis (here the invariant direction) in the topological sense. Therefore, a 2D or 2.5D (which means that B_z is nonzero) treatment is reasonable and provides a sufficiently accurate approximation with respect to the physical insights. The advantage of 2D and 2.5D equilibria is that a widespread number of classes of magnetic configurations can be computed based on the well-known Grad–Shafranov (or, equivalently, Lüst–Schlüter) theory (see Lüst & Schlüter 1957; Shafranov 1958). According to this theory, one needs to solve the equilibrium condition

$$\Delta A = -\frac{d}{dA}\left(p_S + \frac{B_{zS}^2}{2}\right) = -\frac{d\Pi_S}{dA}, \tag{27}$$

which follows from the assumption of translational invariance ($\partial/\partial z \equiv 0$) and the representation of the magnetic field by

$$\boldsymbol{B}_S = \boldsymbol{\nabla} A(x, y) \times \boldsymbol{\nabla} z + B_{zS}(x, y)\boldsymbol{e}_z. \tag{28}$$

Here, B_{zS} is the so-called toroidal component (see, e.g., Moffatt 1978; Schindler 2006); B_{zS} and p_S are necessarily explicit functions of the flux function A. To solve Equation (27), a physically motivated pressure function Π_S has to be defined.

The solutions of Equation (27) are solutions to the MHS equations

$$\boldsymbol{\nabla} p_S = (\boldsymbol{\nabla} \times \boldsymbol{B}_S) \times \boldsymbol{B}_S, \tag{29}$$

$$\boldsymbol{\nabla} \cdot \boldsymbol{B}_S = 0. \tag{30}$$

The two systems of equations (Equations (27)–(28) and Equations (29)–(30)) are equivalent.

The strategy is hence the following. We first need to solve the static Grad–Shafranov equation to obtain an MHS equilibrium suitable to describing solar arcade structures. Then, a reasonable mapping needs to be found that transforms this MHS equilibrium into a stationary state.

3. Results

3.1. Mapping from 2D to Current Sheets Varying in the z Direction

First we want to show that even pure 2D fields can be mapped to stationary fields that depend also on the z direction. A translationally invariant magnetic field can be written as $\boldsymbol{B}_S = \boldsymbol{\nabla} A(x, y) \times \boldsymbol{\nabla} z$, in which the flux function A depends only on x and y and the electric current has only a z component, as is obvious from $\boldsymbol{j}_S \equiv -\Delta A \boldsymbol{e}_z$. A comparison with the definition of the static magnetic field (Equation (11)) then implies that f must be identical to $A(x, y)$ and g to z. With this definition of the magnetic field, the Grad–Shafranov equation that needs to be solved reduces to

$$\Delta A = -\frac{dp_S}{dA}. \tag{31}$$

For the transformation to the stationary magnetic field (Equation (17)), the Poisson bracket has to be evaluated. This is done in the following way:

$$\begin{aligned}[\alpha, \beta]_{f,g} &= \frac{\partial \alpha}{\partial f}\frac{\partial \beta}{\partial g} - \frac{\partial \alpha}{\partial g}\frac{\partial \beta}{\partial f} \\ &= \frac{\partial \alpha(A, z)}{\partial A}\frac{\partial \beta(A, z)}{\partial z} - \frac{\partial \alpha(A, z)}{\partial z}\frac{\partial \beta(A, z)}{\partial A}.\end{aligned} \tag{32}$$

The dependence of the Poisson bracket, and therefore of the Mach number, on z implies that the application of a noncanonical transformation to translationally invariant MHS equilibria creates a magnetic field and a velocity field that can vary in the former invariant direction. From inspection of Equation (17) it is obvious that the geometry of the field lines (and therefore their direction) remains unchanged, while the amplitude of the transformed fields is different from the original one and varies nonlinearly with z.

By exploiting that M_A is an explicit function of the static Euler potentials A and z, the electric current of the transformed field can be evaluated via the relation Equation (18). It results to

$$\begin{aligned}\boldsymbol{j} = &\frac{M_A \frac{\partial M_A}{\partial z}\boldsymbol{\nabla} A - \boldsymbol{e}_z\left(M_A \frac{\partial M_A}{\partial A}(\boldsymbol{\nabla} A)^2\right)}{(1 - M_A^2)^{3/2}} \\ &- \frac{\Delta A\, \boldsymbol{e}_z}{(1 - M_A^2)^{1/2}}.\end{aligned} \tag{33}$$

As A is a function of x and y, it is obvious that the electric current of the transformed field now has components in all three coordinate directions, which also depend nontrivially and nonlinearly on all three coordinates. It is hence quasi-3D, but the field-line structure in each x, y plane is preserved. These additional current components, which are all perpendicular to the magnetic field, guarantee self-consistently that the system is kept in an equilibrium state. Moreover, the current density deviates from the one of the pure 2D MHS field, which has only a current component in the z direction. Hence, despite the fact that we started from an initially highly symmetric configuration, the resulting current displays a much more complex structure.

3.2. Mapping from 2.5D to 3D

The magnetic field of solar arcade structures does not necessarily consist of field lines that lie purely in (x, y) planes laminated in the z direction. Instead, the field lines could possess a helical structure, which means that the magnetic field has a toroidal component pointing in the z direction. Such cases require at least a 2.5D treatment. We refrain here from discussing full 3D scenarios, because they cannot be solved using the Grad–Shafranov theory anymore.

To compute 2.5D MHS equilibria, we need to solve the full Grad–Shafranov Equation (27). The representation of the MHS field via Euler potentials is more tricky in the 2.5D case, because at least one of the Euler potentials has to depend on all three spatial coordinates and must depend linearly on z. Hence, we need to construct such an Euler potential.

The simplest case would be to keep for f the same prescription as in the 2D case, i.e., $f = A(x, y)$, and to assume that g can be defined as $g = z + \tilde{h}(x, y)$. The function $\tilde{h}(x, y)$ can be chosen such that at least locally it can be expressed by the flux function A via $\tilde{h}(x, y) = h(A(x, y), y)$. Such a choice of representation is motivated by the fact that A has the strongest variation in the x direction if the coordinate system is chosen in such a way that the y direction corresponds to the vertical axis of the arcade structures, i.e., it is perpendicular to the solar surface.

While usually the Euler potentials are used to compute the B_{zS} component (e.g., Schindler 2006), this cannot be done so easily anymore for the current representation of the Euler potentials because the function h is not known. Therefore, one needs first to evaluate B_{zS} from the Grad–Shafranov Equation (27), and only then the function h can be determined under some constraints. When comparing the Euler representation for the magnetic field with the representation via the Grad–Shafranov equation

$$\boldsymbol{B}_S = \nabla f \times \nabla g \equiv \nabla A \times \nabla z + B_{zS}\, \boldsymbol{e}_z, \tag{34}$$

it follows that

$$\nabla A \times \nabla h = \nabla A \times \frac{\partial h}{\partial y}\, \boldsymbol{e}_y \equiv B_{zS}(A)\boldsymbol{e}_z. \tag{35}$$

Scalar multiplication of the identity Equation (35) with $\boldsymbol{e}_z$ leads to

$$\left.\frac{\partial h}{\partial y}\right|_{\mathrm{A}} \left.\frac{\partial A}{\partial x}\right|_{y} = -\frac{\partial h}{\partial y}\, B_{yS}(A, y) = B_{zS}(A), \tag{36}$$

where $\frac{\partial A}{\partial x} = -B_{yS}(A, y)$ has to be considered as a function of the chosen coordinates A and y, because the partial differential equation Equation (36) for h has a solution, which is a function of these coordinates.

The function $h(A, y)$ can thus be computed from

$$\begin{aligned} h(A, y) &= -\int \frac{B_{zS}(A)}{B_{yS}(A, y)}\, dy + h_0(A) \\ &= -B_{zS}(A) \int \frac{dy}{B_{yS}(A, y)} + h_0(A). \end{aligned} \tag{37}$$

One should note, however, that the evaluation of the function $h(A, y)$ bears difficulties, for example, if the magnetic field has null points. In that case, $B_{xS}(A, y) = B_{yS}(A, y) = 0$, and $\frac{\partial h}{\partial y}$ diverges. Therefore, to properly define a function $h(A, y)$ in the vicinity of a null point, the toroidal component $B_{zS}(A)$ must be zero on the separatrix surface, i.e., $B_{zS}(A_{\mathrm{sep}}) = 0$ with $\nabla A|_{x_N, y_N} = 0$, if the null point is of the X-point type. In the case of an O-point null point, $B_{zS}(A)$ has to vanish at that point.

To perform the transformation, we recall that the Alfvén Mach number M_{A} is an explicit function of the static Euler potentials $f = A(x, y)$ and $g = z + h(A(x, y), y)$. Equations (36)–(37) provide a representation of these Euler potentials and, therefore, the basis for the definition of M_{A}. Hence, the electric current of the transformed field can be evaluated via the relation Equation (18). It results to

$$\begin{aligned} \boldsymbol{j} &= M_{\mathrm{A}} \frac{\left(\frac{\partial M_{\mathrm{A}}}{\partial A}\nabla A + \frac{\partial M_{\mathrm{A}}}{\partial g}\nabla g\right) \times (\nabla A \times \nabla z + B_{zS}\, \boldsymbol{e}_z)}{(1 - M_{\mathrm{A}}^2)^{3/2}} \\ &\quad + \frac{-\Delta A\, \boldsymbol{e}_z + B'_{zS}(A)\nabla A \times \boldsymbol{e}_z}{(1 - M_{\mathrm{A}}^2)^{1/2}} \end{aligned} \tag{38}$$

$$\begin{aligned} &= M_{\mathrm{A}} \frac{\left(\frac{\partial M_{\mathrm{A}}}{\partial g}\right)\nabla A - \boldsymbol{e}_z\left(\frac{\partial M_{\mathrm{A}}}{\partial A}(\nabla A)^2 + \frac{\partial M_{\mathrm{A}}}{\partial g}\nabla A \cdot \nabla h\right)}{(1 - M_{\mathrm{A}}^2)^{3/2}} \\ &\quad + M_{\mathrm{A}} \frac{\frac{\partial M_{\mathrm{A}}}{\partial A}B_{zS}\nabla A \times \boldsymbol{e}_z + \frac{\partial M_{\mathrm{A}}}{\partial g}B_{zS}\nabla h \times \boldsymbol{e}_z}{(1 - M_{\mathrm{A}}^2)^{3/2}} \\ &\quad + \frac{-\Delta A\, \boldsymbol{e}_z + B'_{zS}(A)\nabla A \times \boldsymbol{e}_z}{(1 - M_{\mathrm{A}}^2)^{1/2}} \end{aligned} \tag{39}$$

$$\begin{aligned} &= \frac{M_{\mathrm{A}}}{(1 - M_{\mathrm{A}}^2)^{3/2}}\left[\left(\frac{\partial M_{\mathrm{A}}}{\partial g}\right)\nabla A \right. \\ &\quad - \boldsymbol{e}_z\left(\left(\frac{\partial M_{\mathrm{A}}}{\partial A} + \frac{\partial M_{\mathrm{A}}}{\partial g}\frac{\partial h}{\partial A}\right)(\nabla A)^2 + \frac{\partial M_{\mathrm{A}}}{\partial g}\frac{\partial h}{\partial y}\frac{\partial A}{\partial y}\right) \\ &\quad \left. + B_{zS}\left(\frac{\partial M_{\mathrm{A}}}{\partial A} + \frac{\partial M_{\mathrm{A}}}{\partial g}\frac{\partial h}{\partial A}\right)\nabla A \times \boldsymbol{e}_z + B_{zS}\frac{\partial M_{\mathrm{A}}}{\partial g}\frac{\partial h}{\partial y}\boldsymbol{e}_x\right] \\ &\quad + \frac{-\Delta A\, \boldsymbol{e}_z + B'_{zS}(A)\nabla A \times \boldsymbol{e}_z}{(1 - M_{\mathrm{A}}^2)^{1/2}} \end{aligned} \tag{40}$$

$$\begin{aligned} &= \frac{M_{\mathrm{A}}}{(1 - M_{\mathrm{A}}^2)^{3/2}}\left[\left(\frac{\partial M_{\mathrm{A}}}{\partial g}\right)\nabla A \right. \\ &\quad - \boldsymbol{e}_z\left(\left(\frac{\partial M_{\mathrm{A}}}{\partial A} + \frac{\partial M_{\mathrm{A}}}{\partial g}\frac{\partial h}{\partial A}\right)(\nabla A)^2 - \frac{\partial M_{\mathrm{A}}}{\partial g}B_{zS}\frac{B_{xS}}{B_{yS}}\right) \\ &\quad + B_{zS}\left(\frac{\partial M_{\mathrm{A}}}{\partial A} + \frac{\partial M_{\mathrm{A}}}{\partial g}\frac{\partial h}{\partial A}\right)\nabla A \times \boldsymbol{e}_z \\ &\quad \left. - B_{zS}\frac{\partial M_{\mathrm{A}}}{\partial g}\frac{B_{zS}}{B_y}\boldsymbol{e}_x\right] + \frac{-\Delta A\, \boldsymbol{e}_z + B'_{zS}(A)\nabla A \times \boldsymbol{e}_z}{(1 - M_{\mathrm{A}}^2)^{1/2}}. \end{aligned} \tag{41}$$

As before (Section 3.1), the variations of the current are induced by the flow, which itself is generated by the noncanonical mapping.

The most interesting result is the occurrence of a current component parallel to the poloidal magnetic field component. Such a component does not exist in a 2D mapping of a pure poloidal field[4] and also not in the quasi-laminar regime

[4] For a translationally invariant magnetic field, only x–y components exist in the poloidal plane, and only one "toroidal" component of the current, namely in the z direction, exists.

discussed in Section 3.1, where only an additional component in the ∇A direction exists due to the change of the Mach number in the z direction. This additional poloidal component $\nabla A \times e_z$ of the current exists not only because of the static component $B'_{zS}(A)\nabla A \times e_z$, but also because of the explicit dependence of M_A on A and g. This latter is true even if the static component B_{zS} is constant.

A current component in the main direction of the (poloidal) magnetic field strengthens the character of the current toward a more field-aligned current. Moreover, it provides the basis for particle acceleration, as a switched-on resistivity would generate an electric field with a strong component parallel to the magnetic field.

3.3. (Non)existence of 3D Force-free Fields

The prerequisites of our investigations on stationary MHD flows and their current structures are MHS equilibria. Force-free states are an important subclass of MHS states. They correspond to states of minimum magnetic energy into which each equilibrium after distortion should relax according to variational calculus (e.g., Sakurai 1979).

The following vivid illustration, which is based on the original ideas of Kippenhahn & Moellenhoff (1975) and Parker (1972), will help to elucidate why force-free states occur. Let us consider that we have a small domain with an interlaced field topology so that one field line is interwoven in such a way that this single field line fills basically the complete volume. Then, by knowing that the pressure is constant along each individual field line,

$$\nabla p_S = (\nabla \times \boldsymbol{B}_S) \times \boldsymbol{B}_S \quad \Rightarrow \quad \boldsymbol{B}_S \cdot \nabla p_S = 0, \tag{42}$$

which is a necessary MHS condition, it follows that the pressure is constant in this whole volume. This leads automatically to a force-free state because $\nabla p_S = (\nabla \times \boldsymbol{B}_S) \times \boldsymbol{B}_S = 0$. In this context, a constant pressure inside the volume hence guarantees that influences from outside are switched off.

In contrast, if the considered field line extends beyond the border of the domain, the condition Equation (42) implies that the pressure inside this volume is, at least partially, determined by constraints from outside (see Parker 1972), and the state is not necessarily force-free.

Recent investigations, allowing at least for field deformations via boundary footpoint displacements, also minimize the influence on the outer boundaries of the MHS environment, such as by the severe assumption that the velocity of the footpoints should vanish at the boundary (see, e.g., Low 2010; Parker 2012). This means that no flow can leave the volume, and any flows that might occur along field lines are basically ignored.

If we were dealing with an exclusively magnetohydrostatic atmosphere where stationary flows could be completely excluded, the force-freeness could be a reasonable assumption. However, as observations have shown, flows are naturally occurring in the solar atmosphere (e.g., Yoshimura et al. 1971; Harvey & Harvey 1976; Wallace et al. 2010) so that the MHS states are embedded in regions in which flows can occur locally. Hence, it is not necessarily always possible to eliminate external influences, but, in contrast, the occurrence of flows can be utilized, because they help to determine exactly the "integral" parameters like the plasma pressure.

We want to test whether or under which circumstances the states after noncanonical transformations can be force-free. For this, we regard the transformation method in analogy to quantum mechanics. The set of equilibria (before and after the transformation) can be considered as a family of stationary states, all having the (geometrically and topologically) identical field-line structure. In this family, the MHS equilibrium defines the ground state ($M_A = 0$, for all x, y, z). All other stationary states with flow can then be regarded as excited states. With this interpretation in mind, there are two possible scenarios for which force-free states can be expected: (1) if the ground state is already force-free, meaning that $\boldsymbol{j}_S \times \boldsymbol{B}_S = \nabla p_S = 0$, or (2) if the original non-force-free ground state turns into a force-free final state when performing the transformation, such as by the application of a flow.

In general, the direction of the magnetic field remains unchanged under the transformation. If we demand that the transformed field be force-free, the following equivalence is valid:

$$\boldsymbol{j} \times \boldsymbol{B} = 0 \Leftrightarrow \boldsymbol{j} \times \boldsymbol{B}_S = 0. \tag{43}$$

After inserting the general form of the transformed current (Equation (18)), the equation on the right-hand side of Equation (43) delivers

$$\frac{\boldsymbol{B}_S^2 \nabla M_A^2}{2(1 - M_A^2)} = \nabla p_S. \tag{44}$$

Let us start with the first case of a force-free ground state. Then Equation (44) implies that $\nabla p_S = 0$. This means that, without loss of generality, M_A must be constant throughout the whole considered domain. This is an extreme constraint for the whole nonlinear MHD flow and is only fulfilled in exceptionally rare cases. A similar result was obtained by Khater & Moawad (2005), who investigated pure 2D nonlinear force-free magnetic fields with mass flow. Field-aligned flows can be regarded as nonlinear perturbation of the MHS state. In analogy to linear perturbation theory, i.e., linear stability analysis, we may say that any unstable mode that might occur will occur. This means that if a self-consistent pressure perturbation,[5] like the one given by Equation (19), will occur (not only at the footpoints of the magnetic field structure), the force-free magnetic field cannot be maintained. Therefore, we can conclude that in any region in which nonlinear flows can occur and are not suppressed, force-free fields will not exist or will vanish.

Turning to the second case, we can decompose the pressure gradient $\nabla p_S = \nabla p_S(f, g)$ and the gradient of the square of the Alfvén Mach number ∇M_A^2 (with $M_A = M_A(f, g)$) in the following way:

$$\frac{\boldsymbol{B}_S^2}{2\,(1 - M_A^2)} \frac{\partial M_A^2}{\partial f} = \frac{\partial p_S}{\partial f}, \tag{45}$$

$$\frac{\boldsymbol{B}_S^2}{2\,(1 - M_A^2)} \frac{\partial M_A^2}{\partial g} = \frac{\partial p_S}{\partial g}. \tag{46}$$

These two equations imply that the expression $\boldsymbol{B}_S^2$ must be an explicit function of f and g only, and hence $\boldsymbol{B}_S^2$ as well as $\boldsymbol{B}^2$ must be constant along field lines. An additional restriction is introduced by the fact that for a given MHS equilibrium (defined by B_S, p_S) two first-order differential equations result

[5] Here, self-consistent means that the pressure variation supports the field-aligned equilibrium flow.

for *one* function, i.e., M_A. This implies that M_A is an explicit function of $\boldsymbol{B}_S^2$. Considering that M_A^2 represents the ratio between kinetic and magnetic energy density, this causes a strong correlation between the magnitude of the energy partition and the magnetic field strength. Such severe restrictions tremendously limit on the one hand the number of basic eligible MHS equilibria that can be used for such a transformation, and on the other hand also the freedom of choice of reasonable Mach numbers and consequently of the flow. This leads to the conclusion that force-free is not a generic result[6] but will occur only for rare cases with severe constraints.

How can we interpret these findings? As we said earlier, the MHS solutions are in general a small subset of the field-aligned incompressible flows. As we could show in almost every case, any of these flows either destroys the initial force-free property of the magnetic field, or the transformed equilibrium of arbitrary topology and geometry cannot be force-free anymore.

The force-free property is not compatible with an equilibrium flow, having a larger cardinality than the original set of MHS states. We excluded non-field-aligned flows in our investigation, as they do not have this strong affinity to MHS states.

4. Examples

We wish to stress that the equations for the transformation of the current derived in Sections 3.1 and 3.2 are generally valid and are limited to neither a particular initial physical scenario nor a specific flow pattern, determined by M_A. In the following, for pure demonstration purposes, we chose two specific ground states, i.e., MHS states, one for a 2D equilibrium and the other for a 2.5D equilibrium. To each, specific flow patterns are applied, and the transformed current is computed. The Mach number profiles are chosen such that significant current fragmentation is achieved. Current fragmentation is an indispensable physical process for plasma heating applications, such as in the solar corona. We thus pick a physical environment for our model calculations that can be considered representative for (subareas) of coronal arcade structures and loops.

4.1. 2D Scenario

We start from a 2D potential field as a current free MHS state. To simulate the footpoint region of a typical solar arcade or of some other monopolar domain of the magnetic field in the solar atmosphere, we superimpose a line dipole, which is located at the solar surface, and a homogeneous field. Our coordinate system has its origin on the solar surface with the x and z axes being tangential to the surface and the y axis perpendicular.

The field configuration is computed from the complex potential $\mathcal{A}(u)$ with $u = x + iy$ and

$$\mathcal{A}(u) = iu - \frac{0.6i}{u}, \tag{47}$$

[6] The force-free paradigm for the solar corona plasma was also criticized by Peter et al. (2015) based on different physical aspects.

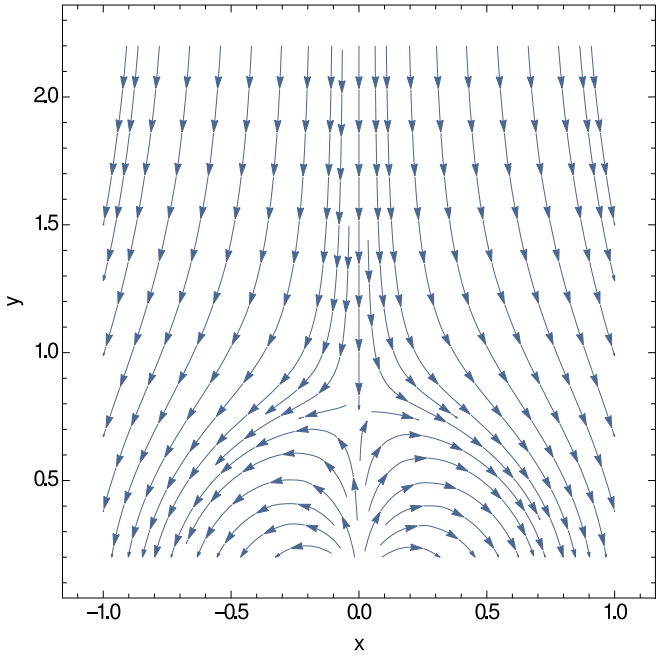

Figure 1. 2D potential field zoomed-in to the dipole region.

where the imaginary part of $\mathcal{A}$ is the magnetic flux function A:

$$\Im(\mathcal{A}) = A(x, y) = x - \frac{0.6x}{x^2 + y^2}. \tag{48}$$

The magnetic field then results to

$$B_{xS} = \frac{\partial A}{\partial y} = -\frac{1.2xy}{(x^2 + y^2)^2}, \tag{49}$$

$$B_{yS} = -\frac{\partial A}{\partial x} = -1 + \frac{0.6y^2 - 0.6x^2}{(x^2 + y^2)^2}. \tag{50}$$

This process delivers an X-type magnetic null point at $(x_N, y_N) = (0, \sqrt{3/5})$ in the upper half domain $y > 0$. For illustration, the field lines of this particular potential field are shown in Figure 1.

The general form of the Mach number profile is given by Equation (23). We chose the function $\mathcal{M}(f, g) \equiv \mathcal{M}(A, z)$ in the following parameterized form:

$$\mathcal{M}(A, z) = \left[\frac{\sin(k_1 A(1 + k_2 z))}{1 + 0.5z^2}\right], \tag{51}$$

where the parameters k_1 and k_2 are constants. The choice of the sine function guarantees that the Mach number profile has a wavy shape, which causes gradients that produce great spatial variations in the resulting current. A nonconstant Mach number that varies spatially on small scales is motivated by the analogy to perturbation theory. Every flow induced by the Mach number should optimize the current distribution to guarantee efficient dissipation of magnetic energy in the form of ohmic heating.

To study the influence of the choice of the Mach number profile on the resulting current structure, we compute two scenarios: one of them is symmetric with respect to the $z = 0$ plane, and the other one asymmetric. For the first, symmetric case, we set $k_1 = 1.57$ and $k_2 = 0$. With these values, the Mach number profile, which is shown in Figure 2, has a very smooth,

only mildly varying shape. Application of this Mach number profile to the MHS state results in the formation of quasi-3D tube-like current filaments. A selection of current isocontours of these filaments is depicted in the bottom panel of Figure 2. The current of this MHD flow has a 3D character, as can be seen in the middle panel of Figure 2, where we plot the current density vector. The current density is strongest in the vicinity of the dipole field and around $z = 0$.

For the second example, we use the following values for the constants in Equation (51): $k_1 = 1.57$ and $k_2 = 0.75$. The resulting Mach number profile is depicted in the top panel of Figure 3, and the isocontours of the current filaments and the current density vector are shown in the bottom and middle panels of Figure 3, respectively. The choice of $k_2 \neq 0$ results in an asymmetry with respect to the $z = 0$ plane in the Mach number profile. In addition, the profile displays clearly stronger gradients. This leads to currents with very narrow, highly filamentary structures, as can be seen in the image of the isocontours.

4.2. 2.5D Scenario

For the 2.5D scenario, we start from a linear force-free field as initial MHS equilibrium. Such fields are typically chosen to model coronal magnetic fields (see the review by Wiegelmann & Sakurai 2012). We restrict our investigation to constant force-free fields, which means that the electric current density is given by $\boldsymbol{j} = c\boldsymbol{B}$, where c is a constant, and we represent our force-free field with the Euler potentials f and g:

$$\boldsymbol{B}_S = \boldsymbol{\nabla} f \times \boldsymbol{\nabla} g, \tag{52}$$

$$f = B_0 \cos(kx) \exp(-\nu y), \tag{53}$$

$$g = z + \frac{c}{\nu} x, \tag{54}$$

where $\nu = \sqrt{k^2 - c^2}$. For the presented case, we fix the constants at the following values: $B_0 = 1$, $k = 1.3$, and $c = 1.2$.

We chose the Euler potentials such that f represents a component of the Fourier expansion of this force-free field (see, e.g., Wiegelmann 1998), and the second term of g describes the component of the field in the z direction, i.e., the toroidal component, where z is chosen as the invariant direction. The force-free magnetic field is shown in Figure 4, where we plot its direction and strength (top panel) and the projection of the field lines into the x–y plane (bottom panel). The magnetic field is strongest for $y = 0$ and decays with increasing values of y. Consequently, the current density also has its maximum at $y = 0$. Moreover, with the chosen representation of the Euler potentials, the current density is a pure function of y and decays exponentially. Selected isocontours of this initial current density are shown in the top panel of Figure 5. Obviously, the isocontours are parallel to the x–z plane, and the maximum value of the current density is reached for $y = 0$, where it has a numerical value of 1.56.

We define the Mach number profile in the following form,

$$M_A = \tanh[\sin(2.5fg)], \tag{55}$$

to provide a spatially strongly oscillating function. It is shown in the middle panel of Figure 5. The results from applying this profile to the static equilibrium are shown in the bottom panel of Figure 5. Obviously, the former isocontour planes of the current density now display wavy structures with dependency

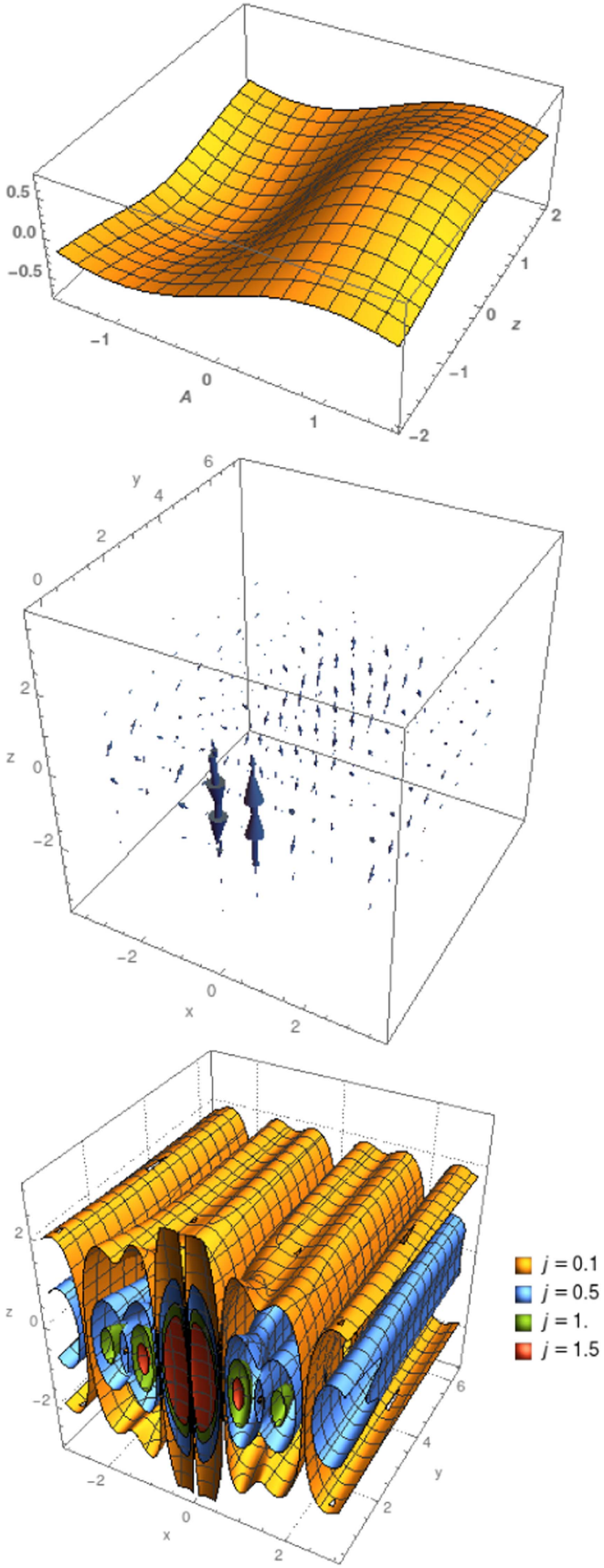

Figure 2. Mach number profile (top) for the values of $k_1 = 1.57$ and $k_2 = 0$ plotted over the phase space $f \equiv A(x, y)$ and $g \equiv z$, current density vectors (middle), and isocontours of the current (bottom) for this Mach number profile.

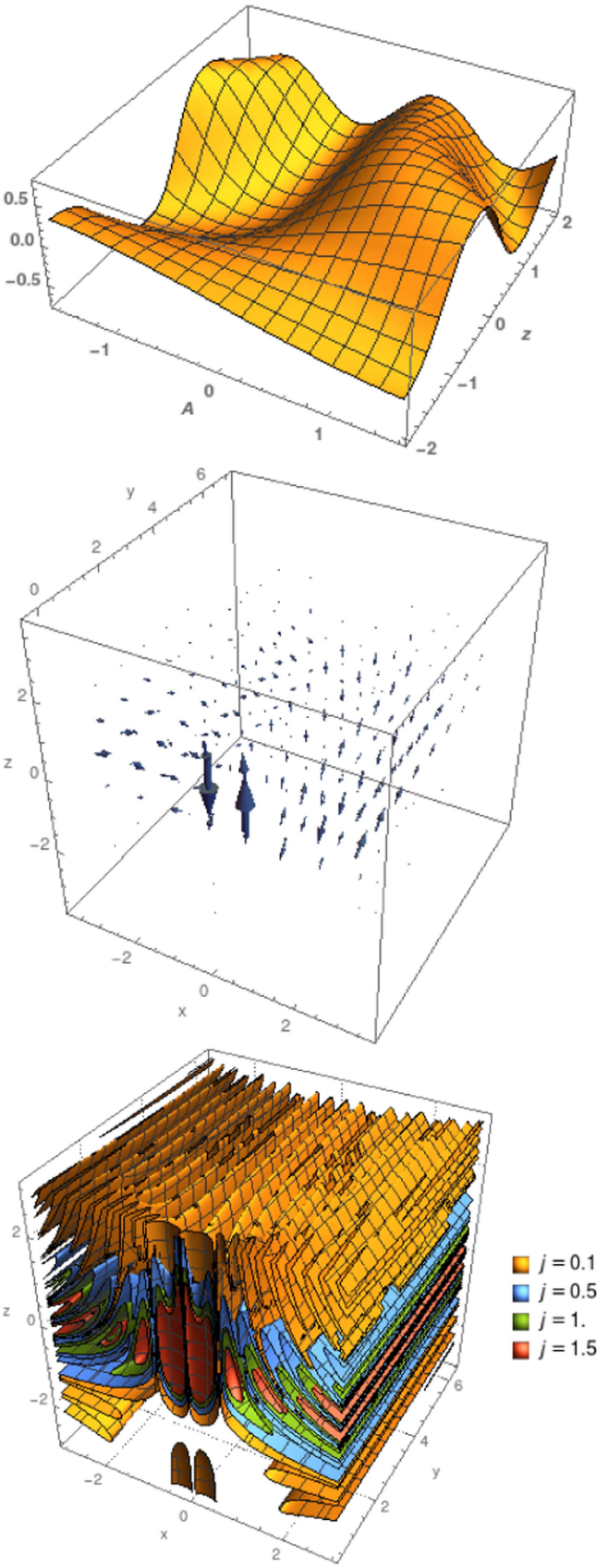

Figure 3. Mach number profile (top) for the values of $k_1 = 1.57$ and $k_2 = 0.75$ plotted over the phase space $f \equiv A(x, y)$ and $g \equiv z$, current density vectors (middle), and isocontours of the current (bottom) for this Mach number profile.

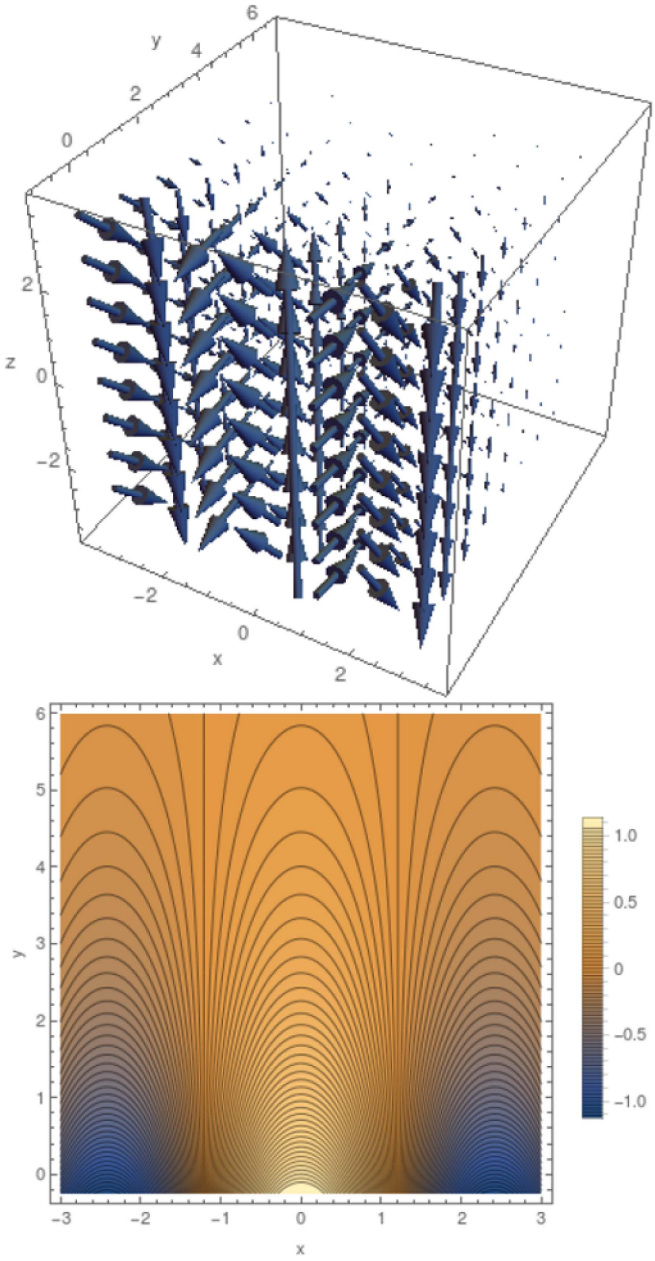

Figure 4. Direction and strength of the initial force-free magnetic field (top) and the projection of the field lines of this field (bottom) into the x–y plane in the 2.5D case. The color coding refers to magnetic flux (function).

in the initially invariant direction, and their surfaces are enlarged. Moreover, the numerical values of the mapped current density are larger, especially in the regions of high initial values of the magnetic field strength. These properties of the mapped current density (enlargement of both the isocontour surfaces and their numerical values) favor such configurations for ohmic dissipation.

5. Discussion and Conclusions

We present a general parameterization for the calculation of noncanonical transformations in the sub-Alfvénic case. This parameterization provides an ideal tool to calculate all possible transformations for a given MHS equilibrium, represented by

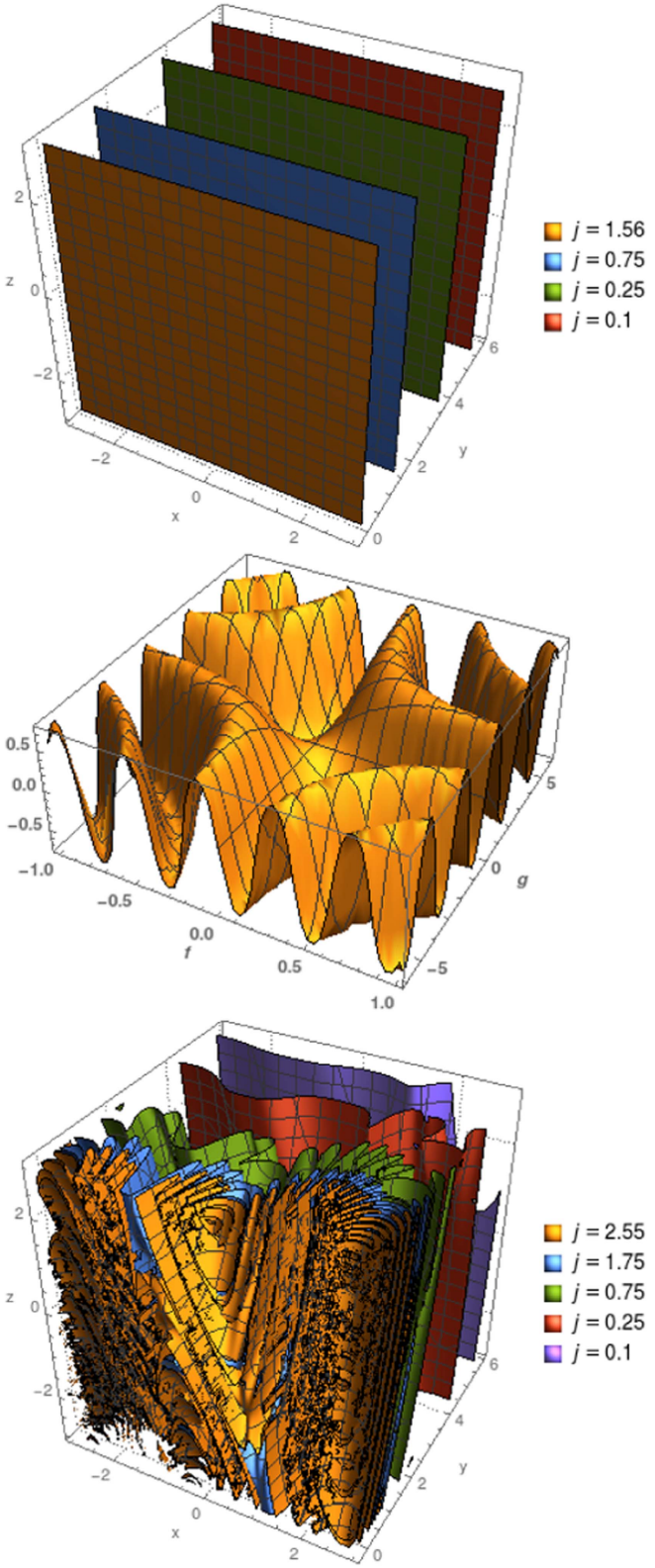

Figure 5. Isosurfaces of the initial current density (top) and Mach number profile (middle), and isosurfaces of the transformed current density (bottom) in the 2.5D case.

the Euler potentials f and g. We apply this parameterization on 2D and 2.5D MHS equilibria and obtain symmetry breaking of the current, resulting in three current components depending on all three spatial coordinates. The symmetry breaking implies that the magnetic field lines can have high symmetry and are ordered and nonchaotic (nonergodic), but due to strong gradients of the flow the current distribution appears strongly shredded, displaying complex lamination. The additional fragmentation of the current filaments from Figure 2 into the highly filamentary structures seen in Figure 3, which is caused by only a slight change in the Mach number profile, shows that it is possible to obtain highly complex current distributions from an initially stationary and ordered magnetic field. These results demonstrate that, to achieve strong currents, it is sufficient to have ordered fields and ordered flows. These currents are in principle suitable for triggering magnetic reconnection or pure ohmic heating. Moreover, our results imply that, in contrast to Parker's idea of coronal heating, pure singular current sheets, i.e., tangential discontinuities, are not necessarily required. It is sufficient to have current sheets that are strong enough to overcome instability thresholds for magnetic reconnection or to achieve the required ohmic heating rates. Such currents can easily be achieved with our model of symmetry breaking. However, it would be desirable to obtain those current density distributions that have sufficient strength and a suitable structure at the right locations to trigger current-driven instabilities. For this, an optimization procedure for the Mach number profile needs to be developed.

Another aspect of our studies is devoted to the question whether force-free fields are generic. Although flows supporting force-free states were a subject of investigation already in the 1970s (Sreenivasan 1973; Sreenivasan & Thompson 1974), only a limited set of such flows could be calculated. However, these flows must obey very specific conditions, which means that the force-free state is not arbitrarily free, and even the force-free parameter α has to obey severe restrictions. As an example, Sreenivasan & Thompson (1974) found that for axis-symmetric cases α must be a function of space and time, while recent studies of Paccagnella & Guazzotto (2011) revealed that confined solutions that necessarily need a monotonically decreasing pressure cannot exist.

Our analysis confirms and reinforces these previous findings. Moreover, it shows that force-free magnetic fields can be maintained by flows either only for specific geometries or for constant Mach numbers.

We thank the anonymous referee for his or her comments and suggestions. This research has made use of NASA's Astrophysics Data System Bibliographic Services (ADS) and was supported from GA ČR under grant numbers 16-05011S and 16-13277S. The Astronomical Institute Ondřejov is supported by the project RVO:67985815. This work was also partly supported by the European Union European Regional Development Fund, project "Benefits for Estonian Society from Space Research and Application" (KOMEET, 2014-2020. 4. 01. 16-0029).

References

Bingert, S., & Peter, H. 2011, A&A, 530, A112
Bogoyavlenskij, O. I. 2001, PhLA, 291, 256
Bogoyavlenskij, O. I. 2002, PhRvE, 66, 056410
Bourdin, P.-A., Bingert, S., & Peter, H. 2013, A&A, 555, A123
Cicogna, G., & Pegoraro, F. 2015, PhPl, 22, 022520
Gebhardt, U., & Kiessling, M. 1992, PhFlB, 4, 1689
Grad, H., & Rubin, H. 1958, in Proc. Second United Nations Int. Conf. Peaceful Uses of Atomic Energy 31, Theoretical and Experimental Aspects

of Controlled Nuclear Fusion, ed. J. H. Martens et al. (Geneva: United Nations Publication), 190
Hansteen, V., Guerreiro, N., de Pontieu, B., & Carlsson, M. 2015, ApJ, 811, 106
Harvey, K. L., & Harvey, J. W. 1976, SoPh, 47, 233
Jelínek, P., Karlický, M., & Murawski, K. 2015, ApJ, 812, 105
Khater, A. H., & Moawad, S. M. 2005, PhPl, 12, 052902
Kippenhahn, R., & Moellenhoff, C. 1975, Elementare Plasmaphysik (Mannheim: Bibliographisches Institut)
Kotrč, P., Bárta, M., Schwartz, P., et al. 2013, SoPh, 284, 447
Leake, J. E., Linton, M. G., & Antiochos, S. K. 2014, ApJ, 787, 46
Low, B. C. 1982, ApJ, 263, 952
Low, B. C. 1985, SoPh, 100, 309
Low, B. C. 1991, ApJ, 370, 427
Low, B. C. 2010, ApJ, 718, 717
Lüst, R., & Schlüter, A. 1957, ZNatA, 12, 850
Manchester, W. 2003, JGRA, 108, 1162
Marsch, E., Wiegelmann, T., & Xia, L. D. 2004, A&A, 428, 629
Moffatt, H. K. 1978, Magnetic Field Generation in Electrically Conducting Fluids (Cambridge: Cambridge Univ. Press)
Neukirch, T. 1995, A&A, 301, 628
Neukirch, T. 1997, A&A, 325, 847
Nickeler, D. H., Goedbloed, J. P., & Fahr, H.-J. 2006, A&A, 454, 797
Nickeler, D. H., Karlický, M., Wiegelmann, T., & Kraus, M. 2013, A&A, 556, A61
Nickeler, D. H., Karlický, M., Wiegelmann, T., & Kraus, M. 2014, A&A, 569, A44
Nickeler, D. H., & Wiegelmann, T. 2010, AnGeo, 28, 1523
Nickeler, D. H., & Wiegelmann, T. 2012, AnGeo, 30, 545
Paccagnella, R., & Guazzotto, L. 2011, PPCF, 53, 095013
Parker, E. N. 1972, ApJ, 174, 499
Parker, E. N. 1983a, ApJ, 264, 642
Parker, E. N. 1983b, ApJ, 264, 635
Parker, E. N. 1988, ApJ, 330, 474
Parker, E. N. 2012, ASSP, 33, 3
Parnell, C. E., & de Moortel, I. 2012, RSPTA, 370, 3217
Peter, H., Warnecke, J., Chitta, L. P., & Cameron, R. H. 2015, A&A, 584, A68
Petrie, G. J. D., & Neukirch, T. 1999, GApFD, 91, 269
Petrie, G. J. D., Tsinganos, K., & Neukirch, T. 2005, A&A, 429, 1081
Petrie, G. J. D., Vlahakis, N., & Tsinganos, K. 2002, A&A, 382, 1081
Pongkitiwanichakul, P., Cattaneo, F., Boldyrev, S., Mason, J., & Perez, J. C. 2015, MNRAS, 454, 1503
Prior, C., & Yeates, A. R. 2016, A&A, 587, A125
Sakurai, T. 1979, PASJ, 31, 209
Schindler, K. 2006, Physics of Space Plasma Activity (Cambridge: Cambridge Univ. Press)
Shafranov, V. D. 1958, JETP, 6, 545
Solov'ev, A. A., & Kirichek, E. A. 2015, AstL, 41, 211
Sreenivasan, S. R. 1973, Phy, 67, 323
Sreenivasan, S. R., & Thompson, D. L. 1974, Phy, 78, 321
Stern, D. P. 1970, AmJPh, 38, 494
Švanda, M., & Karlický, M. 2016, ApJ, 831, 9
Toriumi, S., Iida, Y., Bamba, Y., et al. 2013, ApJ, 773, 128
Tsinganos, K., Surlantzis, G., & Priest, E. R. 1993, A&A, 275, 613
Tsinganos, K. C. 1982, ApJ, 259, 832
Wallace, A. J., Harra, L. K., van Driel-Gesztelyi, L., Green, L. M., & Matthews, S. A. 2010, SoPh, 267, 361
Wiegelmann, T. 1998, PhST, 74, 77
Wiegelmann, T., & Sakurai, T. 2012, LRSP, 9, 5
Wiegelmann, T., Xia, L. D., & Marsch, E. 2005, A&A, 432, L1
Wilmot-Smith, A. L., Pontin, D. I., Yeates, A. R., & Hornig, G. 2011, A&A, 536, A67
Winebarger, A. R., DeLuca, E. E., & Golub, L. 2001, ApJL, 553, L81
Winebarger, A. R., Warren, H., van Ballegooijen, A., DeLuca, E. E., & Golub, L. 2002, ApJL, 567, L89
Yoshimura, H., Tanaka, K., Skimizu, M., & Hiei, E. 1971, PASJ, 23, 443